Time evolution and energy deposition for ion clusters injected into magnetized two-component plasmas

Zhang-Hu Hu, Yuan-Hong Song, and You-Nian Wang*

School of Physics and Optoelectronic Technology, Dalian University of Technology, Dalian 116024, People's Republic of China

(Received 4 August 2011; revised manuscript received 18 December 2011; published 13 January 2012)

A two-dimensional particle-in-cell simulation model is proposed to study the time evolution and energy deposition for ion clusters injected into magnetized two-component plasmas. The injection of an isolated ion cluster is studied in the case of weak and strong magnetic fields. For strong magnetic fields, the ions tend to deposit their energy smoothly along the trajectory of the cluster, due to the confinement by the strong magnetic fields. However, in the case of weak magnetic fields, a large amount of energy is deposited by the ions near the initial cluster injection position, where the cluster density is expected to be largest. We attribute these to the influences of interference effects between the cluster ions, which have close relations to the distances between the ions. Furthermore, the influences of various magnetic fields, injection angles, and injection velocities on the time evolution and energy deposition of a beam pulse, which contains several similar ion clusters, are investigated in detail. The influences of different magnetic fields on the beam pulse show similar to that of a single ion cluster. For increasing injection angles, the beam velocity perpendicular to the magnetic field increases, leading to increasing oscillations in the beam trajectory and energy deposition profile. Besides, the amount of energy that transferred from the beam pulse to the plasma increases as the beam injection velocity approaches the electron thermal velocity.

DOI: 10.1103/PhysRevE.85.016402 PACS number(s): 52.40.Mj, 34.50.Bw, 52.25.Xz

I. INTRODUCTION

The interaction of ion beams and plasmas, including the dynamics of beam particles moving through plasmas, the subsequent slowing-down process due to the interaction with the background electrons and ions, has been an interesting topic since the early 1950s, due to their applications, such as the inertial confinement fusion (ICF) driven by ion beams [1–3], and the neutral beam injection (NBI) [4–6] in the magnetically confined fusion plasmas. Especially, it has proven that the NBI is a highly successful means of plasma heating, in which fast injected neutral particles are converted into fast ions within the plasma after impact ionizations and charge exchanges, and the fast ions slow down by transferring their energy and momentum to the plasma.

Firstly, the interaction of single charged particles with plasmas was investigated through theoretical and numerical methods [7–9]. The so-called stopping power and wake field, which have close relation to the energy transferred from the test charged particle to plasma, are studied in detail. These investigations have provided much useful information for the related experiments. For magnetic confinement fusion and the electron cooling process, the magnetic field plays an important role in the interaction process between the charged particle and the plasma [10–15]. In the case of strong magnetic fields, the plasma ion dynamic polarization shows a significant contribution to the test particle energy loss [14] and the wake field excited by the test particle is found to be highly asymmetrical [15].

For intense ion beams or large ion clusters, typically used for plasma heating in magnetic confinement and inertial confinement fusion plasmas, the influences of interactions between the cluster ions should be taken into consideration [16–20]. The influences of two-ion correlation effects on the fast-ion energy deposition profile in a nondegenerate, high-density plasma are investigated by d'Avanzo, Lantano, and Bortignon [17]. It is shown that the two-ion correlation effects in a sufficiently monochromatic, dense ion beam are important in the determination of its stopping power and of the energy deposition profile. Lately, the correlated ion stopping within N clusters of ion debris are calculated as a linear superposition of every available dicluster pair [18]. The considered model has a direct relevance to the plasma phase of the compressed pellet containing the thermonuclear fuel. Besides, the interference effects, which are produced by the dynamical vicinage interactions between beam particles, on the energy loss of ion beams or ion clusters are studied in detail through the dielectric theory [19]. A strong enhancement in the energy loss of ion beam is obtained for intermediate beam or cluster size. Furthermore, scaling laws are provided for the ion beam energy loss in the interaction of intense ion beams or large ion clusters with fusion plasmas.

However, in addition to the interference effects between the cluster ions, the strong magnetic fields, such as in magnetic confinement fusion plasmas, also have significant effects on the beam-plasma interactions process. As one can expect, in the case of strong magnetic field, the wake field excited by foregoing particles is highly asymmetrical due to the strong Lorentz force by the magnetic field. This asymmetrical wake field may show significant effects on the energy deposition of incoming particles. To our knowledge, there are few investigations on the influences of strong magnetic fields on the interaction process. Also, to fully understand the interaction process, a self-consistent model is needed. As in the widely used neutral beam injection (NBI) module NUBEAM [21], the time-dependent deposition and slowing down of fast ions produced by NBI are calculated through the Monte Carlo method, which is, however, not self-consistent in time. We

*ynwang@dlut.edu.cn

thus perform in this paper the self-consistent two-dimensional (2D) particle-in-cell (PIC) simulations to investigate the time evolution and energy deposition of ion clusters injected into magnetized two-component plasmas. The time evolution of an isolated ion cluster energy loss in the case of weak and strong magnetic fields is also calculated. The influences of different magnetic fields, beam injection angles, and beam injection velocities on the cluster evolution and energy deposition are investigated in detail. Coulomb collisions between charged particles are treated with the Nanbu model [22]. The paper is organized as follows. In Sec. II, two-dimensional PIC simulation methods are briefly described. Simulation results are analyzed in detail for an isolated cluster in Sec. III and a beam pulse in Sec. IV. Finally, we give a short summary in Sec. V.

II. PARTICLE-IN-CELL SIMULATION METHODS

Consider a two-dimensional plasma slab model as shown in Fig. 1. The magnetic field B_0 applied in the plasma is homogeneous and directed along the x axis. The simulation region extends spatially from $x = 0$ to $x = L_x$ and from $y = 0$ to L_y. Initially, the plasma of density n_0 is placed between $L_x/6$ and L_x with the other regions be vacuum. The beam ions are injected at the right boundary with an injection angle θ between the ion beam velocity V_b and the direction of magnetic field. A 2D3V electrostatic particle-in-cell (PIC) code is used for the simulations. All the charged particles are considered to move in the x-y plane. The equations of motion for charged particles are

$$\frac{d\mathbf{r}_j^\alpha}{dt} = \mathbf{v}_j^\alpha, \tag{1}$$

$$\frac{d\mathbf{v}_j^\alpha}{dt} = \frac{Z_\alpha e}{m_\alpha}\left(\mathbf{E} + \mathbf{v}_j^\alpha \times \mathbf{B}_0\right), \quad j = 1,2,\ldots,N_\alpha. \tag{2}$$

Here, $\mathbf{r}_j^\alpha$, $\mathbf{v}_j^\alpha$, Z_α, and m_α are the position, velocity, charge, and mass of plasma electrons ($\alpha = e$), ions ($\alpha = p$), and injection cluster ions ($\alpha = i$), respectively. We shall use the subscripts $\alpha = e$ for plasma electrons, $\alpha = p$ for plasma ions, and $\alpha = i$ for cluster ions. The electric field $\mathbf{E} = -\nabla\phi$ is determined by the Poisson's equation

$$\nabla \cdot \mathbf{E} = \frac{\rho}{\varepsilon_0} = \frac{Z_p n_p + Z_i n_i - n_e}{\varepsilon_0}. \tag{3}$$

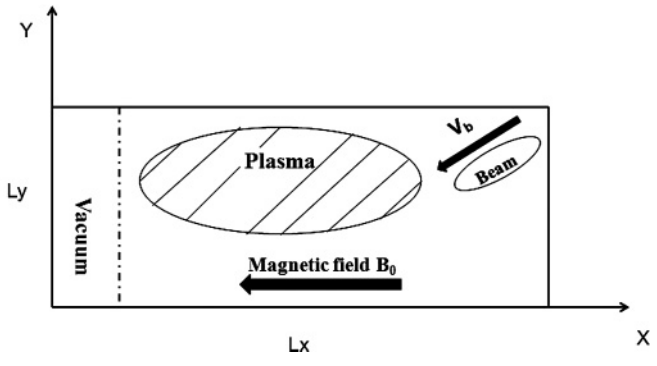

FIG. 1. A two-dimensional plasma slab model.

In our numerical simulations, a hydrogen plasma with mass ratio $m_p/m_e = 1836$ and plasma ion charge $Z_p = e$ is considered. Also the cluster ions are taken to be hydrogen with mass $m_i = 1836m_e$ and charge $Z_i = e$. Plasma parameters used in the simulation are as follows: unperturbed plasma density $n_0 = 5 \times 10^{19}\ \mathrm{m}^{-3}$, initial plasma electron temperature $T_{e0} = 5$ keV, and plasma ion temperature $T_{p0} = 5$ keV. The magnetic field B_0, injection angle θ and cluster injection velocity V_b are treated as variables. Coulomb collisions between electrons, protons, and cluster ions are considered through the Nanbu model [22].

The simulation box is composed of $N_x = 2400$ grids in the x direction and $N_y = 512$ grids in the y direction. The space and time steps are fixed to 7×10^{-5} m and $0.5 - 0.8 \times 10^{-12}$ s for stability. We have adopted averaged 50 superparticles per cell, which has been varied to check the stability of the results. Periodic boundary condition in the y direction and open boundary condition in the x direction are adopted in the simulation. To solve the Poisson's equation, the standard forth and back Fourier transformation is performed in the y direction to introduce a periodicity in this direction. Besides, we have adopted the method developed by Buneman [23] to deal with the open boundary condition in the x direction. The numerical integration of the equations of motion for all charged particles is performed by a standard leapfrog algorithm and the Lorentz forces in Eq. (2) are treated with the Boris rotation [24].

To proceed further it is useful to introduce the following dimensionless variables: $r \to r/\lambda_{\mathrm{De}}$, $v \to v/v_{\mathrm{Te}}$, $t \to t\omega_{\mathrm{Pe}}$, $\phi \to e\phi/k_B T_{e0}$, $n \to n/n_0$, where $\lambda_{\mathrm{De}} = \sqrt{\varepsilon_0 k_B T_{e0}/n_0 e^2}$ is the Debye length of the plasma electrons, $\omega_{pe} = \sqrt{n_0 e^2/\varepsilon_0 m_e}$ the frequency of plasma electrons, $v_{\mathrm{Te}} = \sqrt{k_B T_{e0}/m_e}$ the thermal velocity of plasma electrons, k_B the Boltzmann constant, and T_{e0} the initial electron temperature, respectively.

III. SIMULATION RESULTS FOR AN ISOLATED ION CLUSTER

In the present 2D model, motion in the z direction is allowed and five coordinates are carried for each particle, namely (x, y, V_x, V_y, V_z), which goes partway to a 3D model. The charged particles are considered to move in the x-y plane, with the velocity in z direction V_z also tracked. As we know, the trajectory of charged particles in a magnetic field is a helix. In cylindrical geometry, as shown in Fig. 2, the system can be considered to be axisymmetric. In this configuration, charged particles can be viewed as rotating charged rings subject to guiding center motions parallel and perpendicular to the external magnetic field. Hence, to reduce the computational cost, one can make a 2D particle simulation in the R-Z plane (here R and Z directions represent perpendicular and parallel to the magnetic field B_0, respectively) (i.e., the Y-X plane in our simulation model). The gyration radius and drift motion of charged particles can be obtained in the R direction. In the Z direction, the acceleration and deceleration of charged particles due to the injection of ion beams can be tracked. This configuration has been adopted in Ref. [25] for the simulation of beam focusing experiments and in Refs. [26,27] for beam instability investigations in magnetized plasmas. Furthermore, to validate the present model, we compare the stopping power [in units of $S_0 = (Z_i e)^2/4\pi^2\varepsilon_0\lambda_{\mathrm{De}}^2$] of single

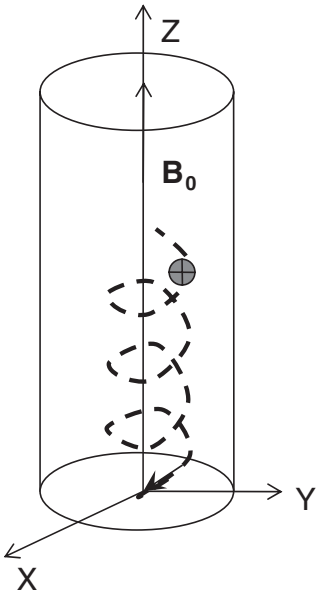

FIG. 2. The trajectory of charged particles in a magnetic field.

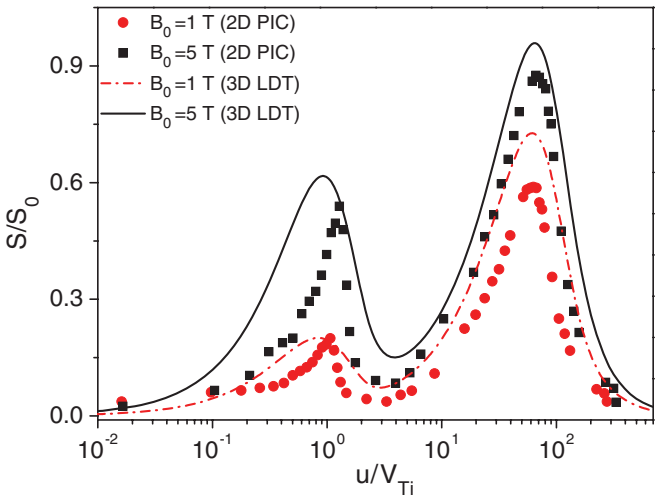

FIG. 3. (Color online) Comparisons of the stopping power [in units of $S_0 = (Z_i e)^2/4\pi^2\varepsilon_0\lambda_{De}^2$] calculated from the present 2D model with that from the solution of linearized Vlasov-Poisson theory [14], which is a full 3D model, for weak and strong magnetic fields.

ions calculated from the present 2D model with that from the solution of the linearized Vlasov-Poisson theory, which is a full 3D model. Detailed information about the solution of the Vlasov-Poisson equation is discussed in Ref. [14], where the energy loss of charged ions in magnetized two-component plasmas is investigated in detail. Comparisons of the stopping power between the two models are made for magnetic fields $B_0 = 1$ T and 5 T in Fig. 3. From the figure, one can see that the results from the two models fit with each other, except for some differences in the magnitude. We attribute this to the limitation of linear theory and some missing information about the wake fields and plasma waves in the present 2D model. Thus, we believe that the present 2D model can give some valuable results for the related experiments and applications. Our further attention will concentrate on a real 3D plasma model in the presence of external magnetic fields.

Note that our main concern here is the influence of magnetic field on the structure evolution of the ion cluster traveling in the magnetized plasma, not only the Larmor radius and the diffusion of charged particles. And the structure of the ion cluster has close relations to the Coulomb force between the cluster ions, the dynamic polarization of background plasma, which is provided to shield the cluster ions and slow down the Coulomb explosions, and the external magnetic field. We first show in Fig. 4 the time evolution of an isolated ion cluster injected into a magnetized plasma with strong magnetic field $B_0 = 5$ T ($\omega_{ce}/\omega_{pe} > 1$, here $\omega_{ce} = eB_0/m_e$ is the cyclotron frequency of plasma electrons), injection angle $\theta = 18^\circ$, and injection velocity $V_b = 0.4v_{Te}$. The ion cluster, which contains about 1.65×10^{14} ions actually, has a Gaussian shape with the length $l_c = 3r_c = 45\lambda_{De}$ and a density of $n_c = 0.3n_0$. In the figure, the densities of the ion cluster (in units of m^{-3}) at three different points in time after injection are displayed. Due to the big differences in the magnitude of cluster density at three different times, the logarithm scale for the cluster density is displayed in the figure. For the strong magnetic field, the injected ions are seen confined very well in the direction perpendicular to the magnetic field and mainly diffuse along the direction of magnetic field lines, as shown in the bottom of Fig. 4. Besides, the travel direction of the ion cluster changes from the initial injection direction to the later direction of the magnetic field lines.

We further show in Fig. 5 the time evolution of the ion cluster in the case of weak magnetic field $B_0 = 1$ T ($\omega_{ce}/\omega_{pe} < 1$) with other parameters the same as Fig. 4. Also, the ion cluster densities (in units of m^{-3}), displayed in the logarithm scale, at three different points in time are shown in the figure. For weak magnetic field, one can see the diffusions of cluster ions along and perpendicular to the magnetic field as the ion cluster penetrates further into the plasma. Due

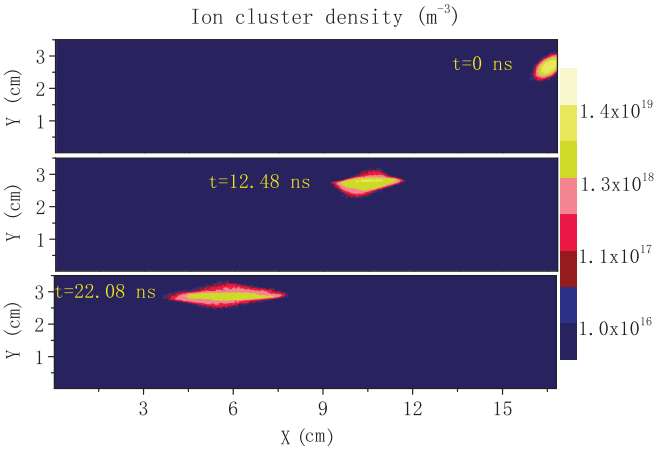

FIG. 4. (Color online) The time evolution of an isolated ion cluster injected into a magnetized plasma with strong magnetic field $B_0 = 5$ T ($\omega_{ce}/\omega_{pe} > 1$, here $\omega_{ce} = eB_0/m_e$ is the cyclotron frequency of plasma electrons), injection angle $\theta = 18^\circ$, and injection velocity $V_b = 0.4v_{Te}$. The cluster densities (in units of m^{-3}) at three different points in time are displayed in the figure. Due to the big differences in the magnitude of cluster density at three different times, the logarithm scale for the cluster density is displayed in the figure.

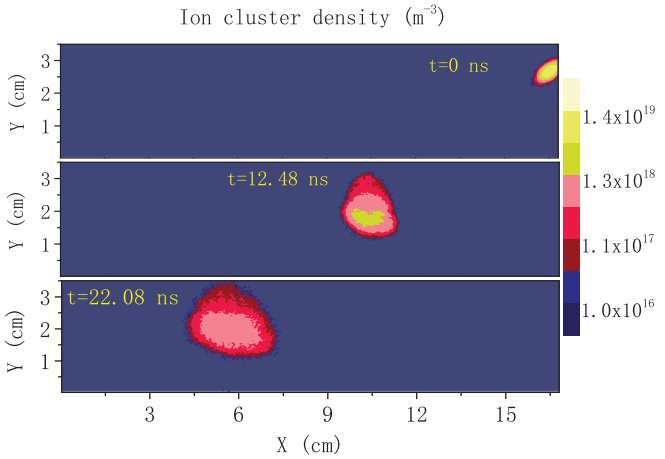

FIG. 5. (Color online) The time evolution of an isolated ion cluster injected into a magnetized plasma with weak magnetic field $B_0 = 1$ T ($\omega_{ce}/\omega_{pe} < 1$), injection angle $\theta = 18°$, and injection velocity $V_b = 0.4v_{Te}$. Also, the densities of ion cluster (in units of m^{-3}), displayed in the logarithm scale, at three different points in time are shown in the figure.

to the Coulomb repulsions between the ions, the density of the ion cluster decreases and the distances between the ions increase gradually. For this reason, the energy transferred from the cluster to the plasma decreases as the cluster travels gradually into the plasma. This can be clearly seen from the corresponding distribution profile of beam energy deposition as shown in Fig. 7, which will be explained in detail in the following.

Also, the corresponding plasma electron densities (in units of m^{-3}) at time $t = 7.68$ ns after ion cluster injection, as described in Figs. 4 and 5, in the case of weak and strong magnetic fields are shown in Fig. 6. In the figure, the plasma and cluster parameters are the same as those in Figs. 4 and 5. The perturbed regions in electron density exerted by the injection ion cluster can be observed, with smaller regions in the strong magnetic field case. In addition, the magnitude of density perturbation in the strong magnetic field case is shown to be stronger than that in the weak magnetic field case, due to the higher ion cluster density, as explained in Figs. 4 and 5.

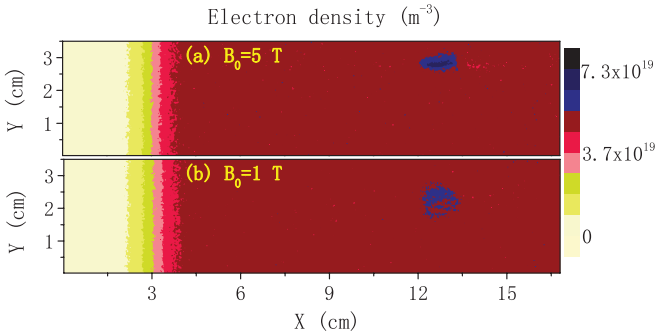

FIG. 6. (Color online) The corresponding plasma electron density (in units of m^{-3}) at time $t = 7.68$ ns after ion cluster injection, as described in Figs. 4 and 5, in the case of weak and strong magnetic fields. The plasma and cluster parameters are the same as those in Figs. 4 and 5.

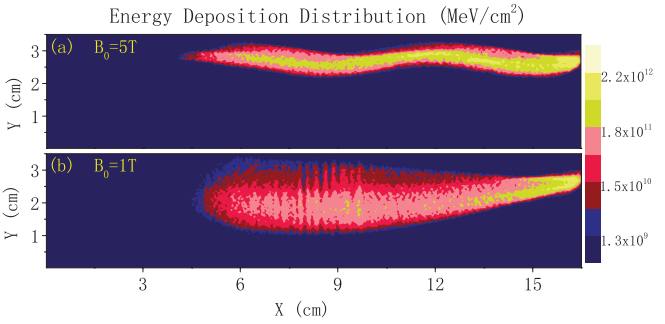

FIG. 7. (Color online) The influences of weak and strong magnetic fields on the distribution profile of cluster energy deposition (in units of MeV/cm^2) at time intervals $t = 22.08$ ns after injection. The other parameters are the same as those used in Figs. 4 and 5.

For particle simulation, we keep track of the position and velocity of cluster ions at every time step. Thus, detailed information about the energy transferred from the cluster ions to the plasma can be obtained. We thus show in Fig. 7 the corresponding distribution profile of cluster energy deposition (in units of MeV/cm^2 for the present 2D model) at time intervals $t = 22.08$ ns after the injection in the case of weak and strong magnetic fields. The total energy deposition, which is given by the integral of distribution profile over the plasma area, is also calculated for different magnetic fields in Fig. 11, which will be explained in the following. The parameters of the plasma and cluster are the same as those in Figs. 4 and 5. As shown in Fig. 7(a) with strong magnetic field $B_0 = 5$ T, the range of cluster ions depositing their energy in the direction perpendicular to the magnetic field is seen to be strongly restricted, due to the strong confinement by the magnetic field. In addition, one can observe the oscillations in the profile of cluster energy deposition. Due to the initial injection angle between the injection velocity and the magnetic field, the cluster has a Larmor radius $r_L \approx \frac{V_\perp}{\omega_{ce}}$ in the y direction while traveling with the speed $V_{//}$ in the x direction at the same time. Here, $V_\perp$ and $V_{//}$ are the velocities of clusters that are perpendicular and parallel to the magnetic field, respectively. For this reason, one thus can observe the oscillations in the energy deposition profile.

In contrast to the strong magnetic field case, the significant increase in the range of cluster energy deposition can be clearly observed in the weak magnetic field case, due to rapid diffusion of the cluster ions. Also, a large amount of beam energy is found to be deposited near the initial cluster injection position, where the cluster density is expected to be largest. As the ion cluster travels gradually into the plasma, the energy transferred to the plasma decreases rapidly due to the Coulomb repulsion between the ions in the cluster, as explained in Fig. 5. Through the comparisons between the weak and strong magnetic field case, one can clearly find that as the magnetic field increases, the ions tend to deposit their energy smoothly along the trajectory of the cluster, as shown in Fig. 7(a). For strong magnetic field, the distances between the ions of injected cluster increase very slowly due to the well confinement of the magnetic field. However, for weak magnetic field case, the distances between the cluster ions increases rapidly. The influence of interference effects,

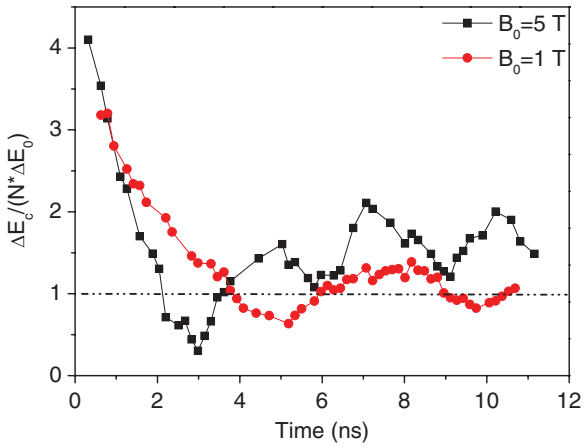

FIG. 8. (Color online) The influences of weak and strong magnetic fields on the time evolution of cluster energy loss $\Delta E_c(t)$, which is calculated through the averaging over clusters of different sizes (different r_c and l_c). For comparison, the energy loss of the cluster $\Delta E_c(t)$ is normalized by $N\Delta E_0$, where N is the number of ions in the cluster and ΔE_0 is the energy loss of single ions.

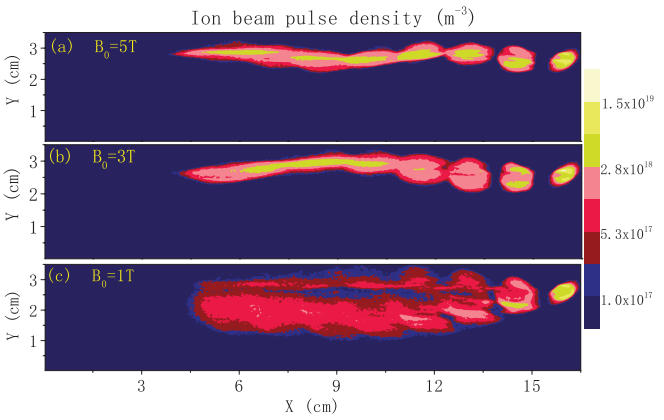

FIG. 9. (Color online) The influences of different magnetic fields on the evolution of an ion beam pulse, which contains several ion clusters, at time $t = 24$ ns with injection angle $\theta = 18^\circ$ and beam velocity $V_b = 0.4v_{\mathrm{Te}}$. The beam pulse densities (in units of m^{-3}) at time $t = 24$ ns in the case of $B_0 = 1$, 3 and 5 T are shown in the figure.

which is closely related to the distances between the ions [17], on the cluster energy deposition decreases rapidly due to this significant increase in the distances. Thus, a rapid decrease and a smooth varying in the energy deposition of weak and strong magnetic fields case, respectively, can be observed in the figure.

To fully understand the energy deposition profile, as shown in Fig. 7, we further investigate in detail the interference effects on the time evolution of cluster energy loss, which is an important quantity for describing the interactions of clusters with the plasma. To clearly show the interference effects, the cluster energy loss, which is calculated through the averaging over clusters of different sizes (different r_c and l_c), is compared with that of single ions in the case of weak and strong magnetic fields, as shown in Fig. 8. In the figure, the cluster energy loss $\Delta E_c(t)$ is normalized by $N\Delta E_0$, where N is the number of ions in the cluster and ΔE_0 is the energy loss of single ions. From the figure, one can see that the energy loss of the cluster is strongly enhanced compared to that of single ions during the initial cluster travel time (about 2 ns) and then shows oscillations near the value of single ions. However, after 4 ns, the cluster energy loss in the strong magnetic field case exceeds that in the weak magnetic field case. From the whole time evolution profile, one thus can expect the rapid decrease in the energy deposition profile of the weak magnetic field case, as already shown in Fig. 7. As the cluster ions diffuse in the plasma and the distances between the ions increase, the energy loss of the cluster approaches that of single ions gradually as the time increases. Also, as the magnetic field increases, the time needed for the cluster energy loss approaching that of single ions increases, as shown in the figure.

IV. SIMULATION RESULTS FOR AN ION BEAM PULSE

As adopted in the neural beam injection experiments in magnetically confined fusion plasmas, the injected beam has a form of pulsed beam. If the time interval between the pulses is short, then the foregoing ion cluster shows the influences on the incoming ion cluster, mainly through the so-called wake field. On the contrary, if the time interval between the pulses is long, then each ion cluster in the beam pulse can be considered to be isolated, showing independence with each other. In addition, investigations are needed to show the influences of pulse width on the traveling and energy deposition of the beam pulse. Thus, we further investigate the time evolution and energy deposition of an intense ion beam pulse, which contains several similar ion clusters, injected into a magnetized plasma. The beam pulse we used in the simulation has a length of 30 ns with a substructure of 334 MHz. Each of these ion clusters has a Gaussian shape with a pulse width of 2.5 ns [full width at half-maximum (FWHM)]. Figure 9 shows the influences of different magnetic fields on the beam pulse density evolution at time $t = 24$ ns with injection angle $\theta = 18^\circ$ and beam injection velocity $V_b = 0.4v_{\mathrm{Te}}$. For the injection time of $t = 24$ ns, the beam pulse shown in the figure contains 8 ion clusters. Similar to that of the single ion cluster, the well confinement of beam pulse by the strong magnetic field and the rapid diffusion of beam ions in the weak magnetic field case can be observed. Also, in the case of the strong magnetic field, the oscillations in the trajectory of beam ions can be found.

Figure 10 shows the influences of different magnetic fields on the energy distribution profile deposited by the beam pulse (in units of $\mathrm{MeV/cm}^2$) with the same parameters as in Fig. 9. The significant increase in the magnitude of beam energy deposition can be clearly observed compared to that of a single ion cluster. The distribution profile of energy deposition shows similar to that of a single ion cluster, except in the magnitude. The smooth energy deposition by the beam pulse along the beam trajectory can also be observed as the magnetic field increases. We also calculate in Fig. 11 the total energy deposition, which is given by the integral of distribution profile over the plasma area, of the isolated cluster (shown in Fig. 7) and beam pulse (shown in Fig. 9) for different magnetic fields at time intervals $t = 22.08$ ns after injection. And the number of ion clusters in the beam pulse is eight. Here the total deposition energy of beam pulse and isolated ion cluster are calculated at the same time intervals (i.e., $t = 22.08$ ns).

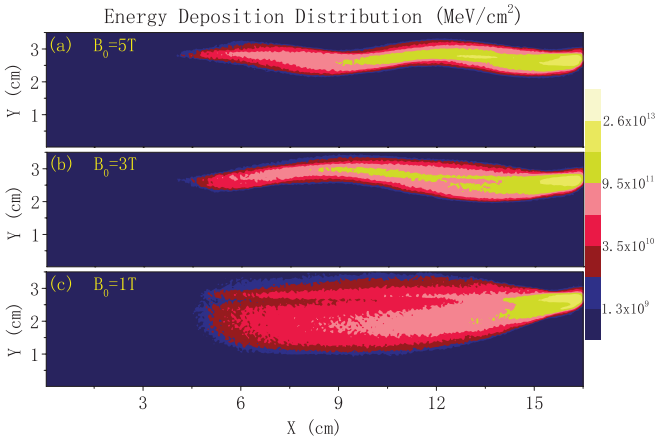

FIG. 10. (Color online) The influences of different magnetic fields on the energy distribution profile deposited by the beam pulse (in units of MeV/cm^2) with the same parameters as in Fig. 9.

During this time interval, the travel distance of each ion cluster in the beam pulse is different, with the largest travel distance for the ion cluster in the front of the beam pulse and the smallest distance for the cluster in the tail of the beam pulse. For example, the eighth ion cluster, in the tail of the beam pulse, just enters the plasma and loses very little energy to the plasma. So, we cannot divide the total deposition energy of beam pulse by the number of ion clusters (i.e., eight) in the beam pulse to obtain the amount of energy deposited per cluster and compare with that of the isolated cluster. In contrast, for each magnetic field strength, we do eight simulations, each simulation with the injection of an isolated cluster, as shown in Figs. 4 and 5. All the simulation parameters, such as plasma parameters,

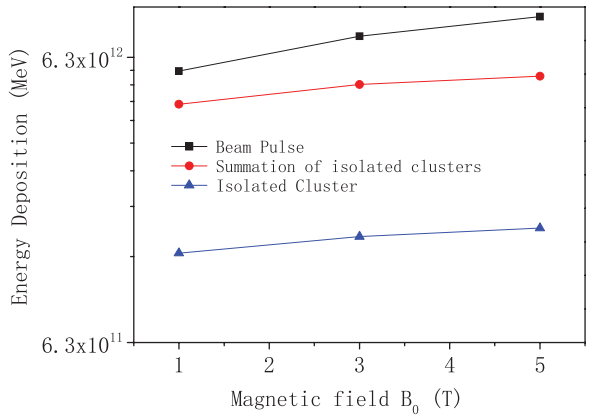

FIG. 11. (Color online) The total energy deposition, which is calculated through the integral of the distribution profile over the plasma area, of the isolated cluster (shown in Fig. 7) and beam pulse (shown in Fig. 9) for different magnetic fields at time intervals $t =$ 22.08 ns after injection. The number of clusters contained in the beam is eight. Also, for each magnetic field strength, the summation of total deposition energy calculated from eight simulations, each simulation with the injection of an isolated cluster as shown in Figs. 4 and 5, is shown in the figure to show comparison between the beam pulse and isolated cluster. All the simulation parameters, such as plasma parameters, cluster size, and velocity, for eight simulations are the same except for the cluster travel distances, which correspond to those of eight ion clusters in the beam pulse, respectively.

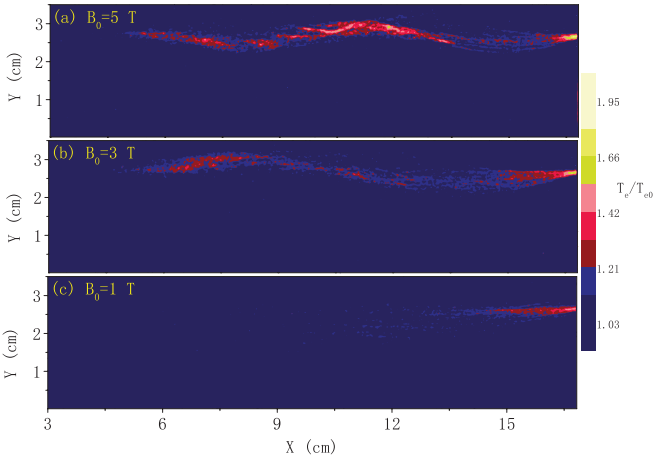

FIG. 12. (Color online) Plasma electron temperature distribution for different magnetic fields at $t = 24$ ns after beam injection with the same parameters as in Fig. 9. The electron temperature T_e shown in the figure is normalized by the initial electron temperature T_{e0} before the beam injection. Besides, the temperature distribution in regions from $x = 0$ to $x = 3$ cm, where plasma electrons diffuse in the vacuum, is not displayed in the figure for clearness.

cluster size, and velocity, for eight simulations are the same expected for the cluster travel distances, which correspond to those of the eight clusters in the beam pulse, respectively. Finally, we sum the total deposition energy calculated from the eight simulations and compare with that of the beam pulse. These summation results are also shown in Fig. 11 (the line with circles). Compared to that of an isolated cluster, the enhancement of the energy deposition produced by the beam pulse can be clearly seen from the figure. For both the isolated cluster and beam pulse, the enhancement in the magnitude of energy deposition with the increasing magnetic field can be observed, which shows accordance with the linear theory [14]. The beam-plasma instabilities (e.g., the two-stream instabilities) play an important role in the energy deposition for the present density ratio of beam to plasma $n_c/n_0 = 0.3$. In this region, plasma heating is dominated by collective beam stopping, in contrast to the classical Coulomb interactions, and a large fraction of beam energy is transferred to the plasma through beam-plasma instabilities. In addition, the collisions between charged particles (e.g., collisions between the ions, plasma electrons, and plasma ions) are also considered here through the Nanbu model [22], which is especially suitable for particle simulation. Detailed information about the influences of beam-plasma instabilities on the ion energy deposition will be presented elsewhere.

Also, the corresponding plasma electron temperature T_e at $t = 24$ ns after beam injection is shown in Fig. 12 for different magnetic fields, with the same parameters as in Fig. 9. The electron temperature T_e shown in the figure is normalized by the initial electron temperature T_{e0} before the beam injection. Besides, the temperature distribution in regions from $x = 0$ to $x = 3$ cm, where plasma electrons diffuse in the vacuum, is not displayed in the figure for clearness. One can see from Fig. 12(c), the case of weak magnetic field, that the plasma electrons are mainly heated near the initial beam injection position, where a large amount of energy is deposited by the

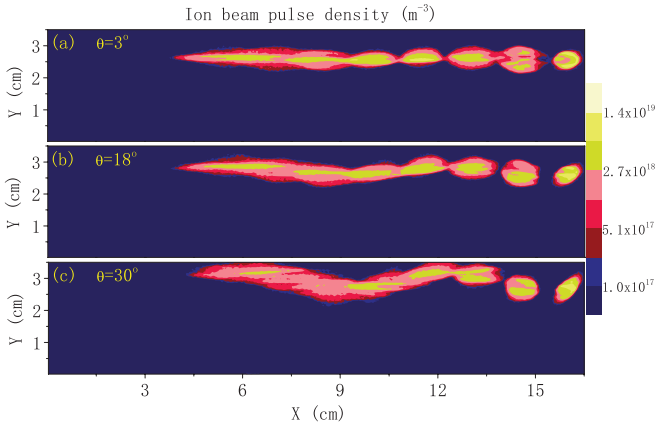

FIG. 13. (Color online) The influences of different injection angles on the density evolution (in units of m^{-3}) of ion beam pulse at time $t = 24$ ns with magnetic field $B_0 = 5$ T and beam velocity $V_b = 0.4v_{\mathrm{Te}}$.

injection beam, as explained in Fig. 10. In other regions, the increase in plasma electron temperature is seen to be limited. At the same time, in the case of strong magnetic fields, the increase in the temperature of plasma electrons along the beam trajectory, not only near the initial beam injection position, can be observed. These show accordance with the conclusions from Fig. 10.

Figure 13 shows the influences of different injection angles on the beam pulse density evolution at time $t = 24$ ns with magnetic field $B_0 = 5$ T and beam velocity $V_b = 0.4v_{\mathrm{Te}}$. The ion beam is confined well along the magnetic field line as the beam penetrates further into plasma. The Larmor radius in the y direction of the beam trajectory is seen to increase as the injection angle increases due to higher beam velocity in the direction perpendicular to the magnetic field. Also, the diffusion of the ion beam is seen to be enhanced as the injection angle increases. These characters can be more clearly observed from the energy distribution profile deposited by the beam pulse as shown in Fig. 14 with the same parameter as in Fig. 13. The increase of beam energy deposition range in the y direction can be clearly observed for large injection angles.

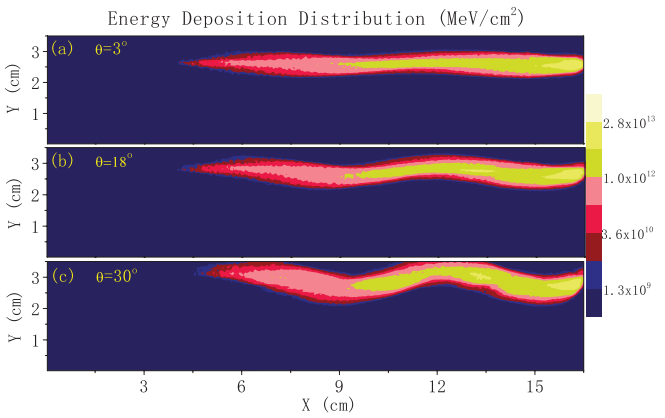

FIG. 14. (Color online) The influences of different beam injection velocities on the energy deposition profile of the beam pulse (in units of MeV/cm^2) with the same parameters as in Fig. 13.

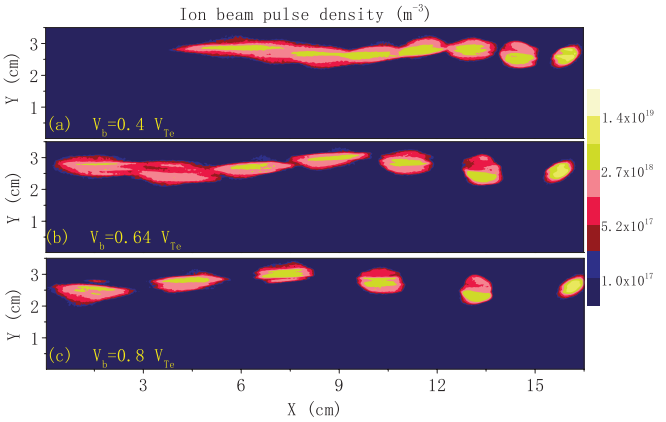

FIG. 15. (Color online) The influences of different beam injection velocities on the density evolution (in units of m^{-3}) of ion beam pulse at time $t = 24$ ns [Fig. 15(a)], $t = 20.16$ ns [Fig. 15(b)], and $t = 16.32$ ns [Fig. 15(c)] with magnetic field $B_0 = 5$ T and injection angle $\theta = 18°$.

Figure 15 shows the influences of different beam injection velocities on the ion beam density evolution at time $t = 24$ ns [Fig. 15(a)], $t = 20.16$ ns [Fig. 15(b)], and $t = 16.32$ ns [Fig. 15(c)] with magnetic field $B_0 = 5$ T and injection angle $\theta = 18°$. The distances between the ion clusters are seen to increase as the beam injection velocity increases. For high beam velocity, the ion clusters of the beam are seen to be independent with each other and the interaction between each cluster is very weak. Also, the corresponding beam energy deposition profile is shown in Fig. 16 with the same parameters as in Fig. 15. In the range $x < 3$ cm, there are no plasma electrons and ions initially. However, as time goes by, the plasma electrons and ions diffuse into this region. As shown in Figs. 16(b) and 16(c), where the beam pulse has a higher injected velocity, the ions in the front of the beam pulse can travel into this region and interact with the plasma electrons and ions here. Also, a diffusion electric field is introduced here due to the diffusion of plasma electrons and ions. So, the energy deposition of the beam pulse in this region can be observed in Figs. 16(b) and 16(c). From the figure, one can see that the amount of energy transferred from the beam ions to the

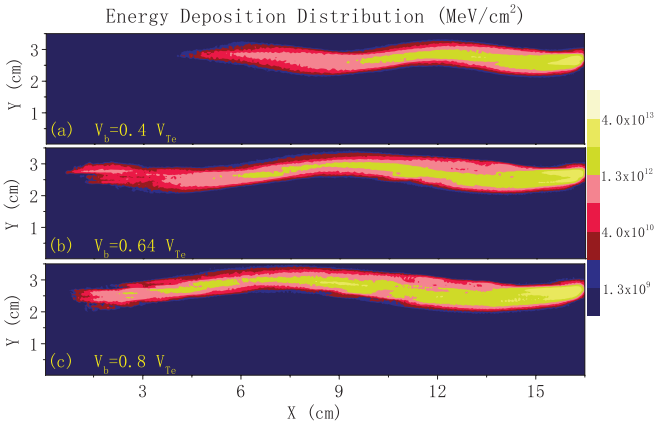

FIG. 16. (Color online) The influences of different injection angles on the energy distribution profile deposited by the beam pulse (in units of MeV/cm^2) with the same parameters as in Fig. 15.

plasma increases as the beam injection velocity V_b approaches the electron thermal velocity V_{Te}.

V. CONCLUSION

Two-dimensional particle-in-cell simulations are performed to investigate the time evolution and energy deposition for ion clusters injected into magnetized two-component plasmas. First, the influences of weak and strong magnetic fields on the time evolution of an isolated ion cluster are investigated. The diffusion of cluster ions and the range of cluster energy deposition in the plasma reduce as the magnetic field increases. Also, the cluster ions tend to deposit their energy smoothly along the trajectory of the cluster due to the well confinement by the strong magnetic fields. However, for the weak magnetic field case, a large amount of energy is deposited by the cluster ions near the initial injection position, where the cluster density is expected to be largest. We attribute these to the influences of interference effects between the cluster ions, which have close relations to the distances between the ions. In the weak magnetic field case, the distances between the cluster ions increases rapidly due to the Coulomb repulsions. To fully understand the energy deposition profile, the interference effects on the time evolution of cluster energy loss are investigated in detail for weak and strong magnetic field cases. Comparing to that of single ions, the cluster energy loss is strongly enhanced during the initial travel time and then shows oscillations near the value of single ions.

Furthermore, the influences of different magnetic fields, injection angles, and injection velocities on the evolution and energy deposition of a beam pulse, which contains several similar ion clusters, are investigated in detail. The influences of various magnetic fields on the beam pulse show similar to that of single ion cluster. For increasing injection angles between the magnetic field and injection velocity, the beam velocity perpendicular to the magnetic field increases, leading to the increasing oscillations in beam trajectory and the distribution profile of energy deposition. In addition, the amount of energy transferred from the beam to the plasma increases as the beam injection velocity approaches the electron thermal velocity.

In this work, we have considered the influences of magnetic fields on the interaction process between the cluster (or beam) and the plasma in a self-consistent way. We believe that the results obtained will provide a helpful reference to the experiments relative to fusion plasmas, such as heating by neutral beam injection. For inertially confined fusion driven by ion beams, the dense plasma density would place the ion cluster plasma interaction in the different regime, where different physics will be involved and a different simulation model would be expected. However, the present studies can still provide some helpful references to the experiments relative to inertially confined fusion plasmas. For example, the conclusions about the influence of interference effects between the cluster ions on the energy deposition, which is an important quality for plasma fusion, can also provide some insights into the beam-plasma interactions in inertially confined fusion plasmas. Our further attention will concentrate on a real 3D and complicated plasma model in the presence of external magnetic fields.

ACKNOWLEDGMENTS

This work is supported by the National Basic Research Program of China (Grants No. 2010CB832901 and No. 2008CB717801), the Fundamental Research Funds for the Central Universities (Grant No. DUT10ZD111), and the Program for New Century Excellent Talents in University (NCET-08-0073).

[1] D. Keefe, Annu. Rev. Nucl. Part. Sci. **32**, 391 (1982).
[2] C. Deutsch, Ann. Phys. Fr. **11**, 1 (1986).
[3] T. Peter and J. Meyer-ter-Vehn, Phys. Rev. A **43**, 1998 (1991).
[4] E. Spetch, Rep. Prog. Phys. **52**, 57 (1989).
[5] E. Thompson, D. Stork, H. P. L. de Esch, Phys. Fluids B **5**, 2468 (1993).
[6] T. Takahashi, T. Kato, and Y. Kondoh, Phys. Plasmas **11**, 3801 (2004).
[7] T. Peter and J. Meyer-ter-Vehn, Phys. Rev. A **43**, 1998 (1991).
[8] C. Couillaud, R. Deicas, Ph. Nardin, M. A. Beuve, J. M. Guihaumé, M. Renaud, M. Cukier, C. Deutsch, and G. Maynard, Phys. Rev. E **49**, 1545 (1994).
[9] G. Zwicknagel, C. Toepffer, and P.-G. Reinhard, Phys. Rep. **309**, 117 (1999).
[10] H. B. Nersisyan, Phys. Rev. E **58**, 3686 (1998); H. B. Nersisyan and C. Deutsch, Phys. Lett. A **246**, 325 (1998).
[11] C. Cereceda, C. Deutsch, M. De Peretti, M. Sabatier, and H. B. Nersisyan, Phys. Plasmas **7**, 2884 (2000).
[12] H. B. Nersisyan, G. Zwicknagel, and C. Toepffer, Phys. Rev. E **67**, 026411 (2003).
[13] C. Cereceda, M. De Peretti, and C. Deutsch, Phys. Plasmas **12**, 022102 (2005).
[14] Z.-H. Hu, Y.-H. Song, and Y.-N. Wang, Phys. Rev. E **79**, 016405 (2009).
[15] Z.-H. Hu, Y.-H. Song, and Y.-N. Wang, Phys. Rev. E **82**, 026404 (2010).
[16] C. Deutsch, Laser Part. Beams **8**, 541 (1990).
[17] J. D'Avanzo, M. Lontano, and P. F. Bortignon, Phys. Rev. A **45**, 6126 (1992); Phys. Rev. E **47**, 3574 (1993).
[18] C. Deutsch and P. Fromy, Phys. Rev. E **51**, 632 (1995).
[19] E. M. Bringa and N. R. Arista, Phys. Rev. E **52**, 3010 (1995).
[20] N. R. Arista and E. M. Bringa, Phys. Rev. A **55**, 2873 (1997).
[21] A. Pankin, D. McCune, R. Andre, G. Bateman, and A. Kritz, Comput. Phys. Commun. **159**, 157 (2004).
[22] K. Nanbu, Phys. Rev. E **55**, 4642 (1997).
[23] O. Buneman, J. Comput. Phys. **12**, 124 (1973).
[24] R. W. Hockney and J. W. Eastwood, *Computer Simulation Using Particles* (McGraw-Hill, New York, 1981), Secs. 3.5 and 4.4.
[25] I. D. Kaganovich, E. A. Startsev, A. B. Sefkow, and R. C. Davidson, Phys. Rev. Lett. **99**, 235002 (2007).
[26] H. Okuda, R. Horton, M. Ono, and K. L. Wong, Phys. Fluids **28**, 3365 (1985).
[27] M. V. Goldman, F. Crary, D. L. Newman, and M. Oppenheim, Phys. Plasmas **7**, 1732 (2000).